Journal homepage: http://gwse.iheg.org.cn

Research Article

Water control structure of loess plateau fill slopes: Composite of low-permeability interbedded strata and anti-erosion surface layer

Xiao-chao Zhang[1], Ming-li Li[1*], Lin-wan Chen[1], Xiang-jun Pei[1], Jun-lin Jiang[1], Shan-shan Wang[1,2]

[1] *State Key Laboratory of Geohazard Prevention and Geoenvironment Protection*, *University of Technology*, *Chengdu* 610054, *China*.
[2] *Baoji University of Arts and Sciences*, *Baoji* 721013, *Shaanxi*, *China*.

Abstract: The extensive fill engineering slopes formed by major projects such as "managing the ditch and creating land" in the Loess Plateau region face severe challenges of rainfall-induced instability. Inspired by the self-stable structure of natural loess-paleosol sequences and the Nature-based Solutions (NbS) concept, the water-control structure for loess fill slopes was propose, which is a composite of erosion-resistant surface layer (modified cellulose-treated) and low-permeability layers (mimicking paleosol properties using lime-improved loess). Indoor soil mechanics tests (liquid/plastic limits, compaction, permeability, shear strength) and Scanning Electron Microscopy (SEM) analysis revealed that both modified materials significantly enhance soil strength and reduce permeability (e.g., lime treatment reduced saturated permeability by 95.18%). Artificial rainfall model experiments demonstrated that slopes with water—control structure exhibit delayed infiltration response (up to 1,565 minutes), reduced erosion volume (71.6% less than untreated slopes), and shifted failure modes from fluidized collapse to gradual shear-slip. Numerical simulations (GeoStudio) further optimized the low-permeability layer configuration, identifying a 3 m-thick, 2°-inclined layer as optimal for maximizing stability. This study reveals that the NbS structure effectively regulates rainfall infiltration and erosion processes, significantly reducing erosion volume and altering failure modes. Consequently, the NbS-based water-control structure provides a theoretical basis and key technical support for the prevention and control of instability in loess fill slopes.

Keywords: Loess fill slope; Nature-based Solutions (NbS); Rainfall-induced erosion; Water-control structure; Stability enhancement

Received: 03 Apr 2025/ Accepted: 24 Jan 2026/ Published: 30 Apr 2026

Introduction

The Loess Plateau is not only the core zone of "One Belt One Way" and the key area of western development (Li et al. 2021), but also an area with fragile ecological environment and frequent geological disasters (Yu et al. 2023; Yu et al. 2023; Xiao et al. 1995). The northern Shaanxi Plateau is the central part of the Chinese Loess Plateau, and Yan'an city is located in the middle of the northern Shaanxi Plateau (Xu et al. 2025). In order to relieve the shortage of land in the old city, the local government carried out the "building a city on leveled mountains" plan to fill the loess gully area. In the past 10 years, a new city area of 78.5 km^2 has been built and a large number of engineered fill slopes were generated (Fig. 1a). For the purpose of preventing the headward erosion of rivers on the loess tableland and reducing loess and water loss, the Yan'an government further carried out the project of "consolidating the ditch and protecting the plateau" to fill the gully head area with serious erosion and form a loess fill slope (Fig. 1b). In order to alleviate the problem of the reduction of cultivated land, the government realized the increase of cultivated land area through the project of "managing the ditch and creating

*Corresponding author: Ming-li Li, *E-mail address*: limingli18@cdut.edu.cn

DOI: 10.26599/JGSE.2026.9280080

Zhang XC, Li ML, Chen LW, et al. 2026. Water control structure of loess plateau fill slopes: Composite of low-permeability interbedded strata and anti-erosion surface layer. Journal of Groundwater Science and Engineering, 14(2): 213-232.

2305-7068/© 2026 Journal of Groundwater Science and Engineering Editorial Office This is an open access article under the CC BY-NC-ND license (http://creativecommons.org/licenses/by-nc-nd/4.0)

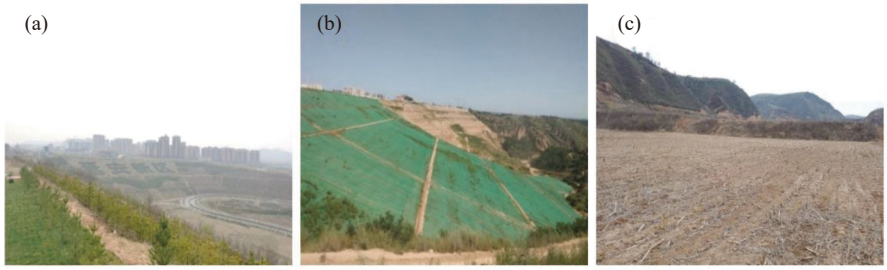

Fig. 1 Filling slopes produced by three managed projects on the loess plateau (a. "building a city on leveled mountain" plan, b. the project of "consolidating the ditch and protecting the plateau", c. warp land dam)

land" and the main engineering measures are to build warp land dams (Fig. 1c). These "super engineering" have produced many loess filling slopes, which not only bring opportunities for urban development, but also pose major geological hazards, which are mainly embodied in the hydraulic erosion effect of rainfall on loess slope.

The loess is characterized by a loose structure, large pores, vertical joint development, strong collapsibility and water sensitivity. Under the priming action of rainfall or irrigation, the strength of the loess will be greatly reduced, which easily causes engineering geological problems such as failure of foundation and slope instability (Konagai et al. 2023; Peng et al. 2020; Zhu et al. 2022). Loess filling engineering has massive geological problems such as deep excavation and high filling, huge filling amount, complex filling materials, fast filling rate, unmanageable compaction degree, complex hydrogeological condition, etc., which make the stability problems of high loess filling slope particularly prominent (Zhao et al. 2025; Cheng et al. 2023). The loess filling slope has the structure of "three sides, two bodies, and one water" (Fig. 2). If the mutual relations among various elements are not controlled and balanced properly, the filling projects will be faced with serious

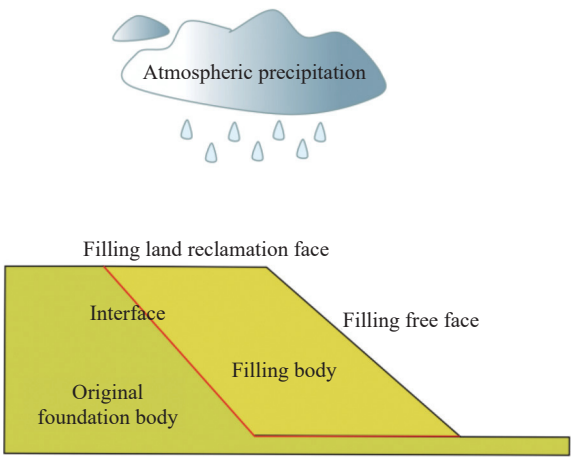

Fig. 2 “Three sides, two bodies and one water structure” of a loess filling engineering slope

potential hazards such as slope instability, slope erosion and damage (Chen et al. 2004). Approximately 95% of landslides are induced by rainfall (Jiang et al. 2023), indicating that rainfall is the most important factor inducing slope catastrophe in loess filling projects (Zhang et al. 2019). The influence of rainfall on the loess slope is concentrated in two aspects: (1) the erosion effect of rainfall on the slope; (2) rainfall infiltration increases the slope unit weight, softens the soil body and reduces the shear strength, which causes the instability of the loess filling slope and leads to landslides (Lu et al. 2023; Tan et al. 2022; Gabet et al. 2006; Hungr et al. 2001). Rainfall infiltration will cause local groundwater level elevation or local saturation layer formation, resulting in wet subsidence, sliding and diffuse failure instability of the loess filling slopes (Ma et al. 2025; Derbyshire et al. 1994; Göksel, 1982). When there is one or more layers of paleosol in the loess slope, it can effectively slow down the infiltration of surface water and has a better water insulation performance (Chen et al. 2024; Li et al. 2024), which makes the loess - paleosol layered structure slope have good self-stability and enable it to stand for decades or even hundreds of years under the action of rainfall (Bao et al. 2022). After adding modified cellulose to the soil of the loess filling slope, the soil erosion resistance performance was significantly improved (Zhang et al. 2021). Although scholars have made considerable progress in the treatment of loess fill slopes, the following problems still exist: First, the coupling mechanism of seepage - stress - deformation has not been fully characterized. Most of the existing studies are single - factor analyses of the permeability coefficient (Zhang et al. 2003), and the evolution patterns of the seepage field, stress field and deformation field of loess fill slopes under rainfall lack systematic quantification (Regmi et al. 2014). Secondly, NbS have gained prominence in geotechnical engineering for their ability to emulate natural systems (Bauduceau et al. 2015). In loess engineering, existing NbS applications primarily focus on surface vegetation (Li et

al. 2020) or isolated soil amendments (Zhang et al. 2021), yet the systematic method of simulating their engineering characteristics and optimizing thier layout parameters (such as the number of layers and dip angle) through artificial materials (such as lime - stabilized layers) is still not mature. To break through these bottlenecks, it is necessary to integrate multi - scale research methods such as microscopic characterization (such as SEM electron microscopy analysis), field experiments and numerical simulation, in order to connect the NbS implementation path of "mechanism revelation - technology optimization - engineering implementation".

To address critical gaps in NbS application, particularly the quantification of seepage - stress - deformation coupling under rainfall and optimized layer configuration, this study integrates multi-scale methodologies: (1) Indoor soil mechanics tests (liquid/plastic limits, compaction, permeability, shear strength) and SEM analysis quantify the enhanced engineering properties of lime/cellulose - modified loess, establishing the material basis for subsequent simulations; (2) the artificial rainfall model test verifies the hydraulic performance of slopes with and without water control structures, the failure mode of the slope body under rainfall, and provides reliable data for the calibration of numerical models; (3) GeoStudio conducts a systematic stability analysis of different low-permeability layer structures (thickness, dip angle) by measuring parameters through indoor geotechnical experiments, and combined the optimization of water control structure design with engineering implementation. Theoretically, the study clarifies the hydraulic seepage and deformation mechanism of the water-control structure of loess fill slopes based on NbS under the action of rainfall. Practically, it offers eco-friendly, cost-effective strategies for landslide prevention in Loess Plateau region of China, supporting sustainable development and ecological conservation in the Yellow River Basin. This NbS- to-engineering translation bridges natural resilience principles with actionable geotechnical solutions.

1 The water-control structure of loess filling slope based on nature-based solution was proposed

The Nature-based Solutions (NbS) refer to solutions that are inspired by nature, support nature, or emulate nature to solve one or more challenges, and are methods that conform to the laws of nature, sustainable and green development (Bauduceau et al. 2015). The mixed layers of illite/montmorillonite (I/S) in paleosol have high mineral content, fine particle composition, and high clay particle content. The soil is relatively dense, and the particles are mostly touched by edges or wrapped in clay. The fine particles are filled in large pores, which makes the structure more stable, the soil strength higher, and the engineering properties better. The paleosol layer can slow down the water migration velocity in loess and has an obvious water-resisting effect, and the loess-paleosol layer structure has good self-stability (Fig. 3). The soil anti-erosion characteristics can be improved effectively by using the new loess curing agent of modified cellulose. Based on the NbS concept, a water-control structure was proposed in the disaster prevention and control of loess filling slope, namely: in the process of filling and building of the loess filling slope, the loess was modified by lime to form a low-permeability layer, defined as an artificial barrier designed to mimic the water-resisting function of natural paleosol layers. One to multiple low-permeability layers were laid in the slope to further form a self-stable structure similar to the loess-paleosol interbedded strata (Zhang et al. 2022). The new loess curing agent was added to the slope surface soil to form an erosion - resistant surface layer (Fig. 4). As shown in Fig.4a, the overall structure comprises an anti-erosion surface layer and internal low-permeability layers. Fig.4b provides a detailed view of a single low-permeability layer mimicking the paleosol.

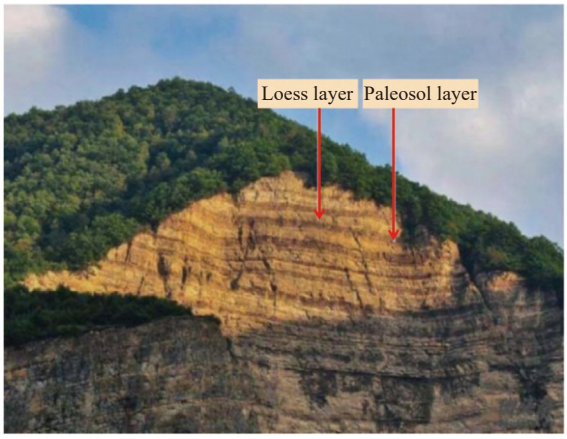

Fig. 3 Loess-paleosol self-stable structure

2 Experimental study on engineering characteristics of remolded loess and improved loess

2.1 The remolded loess

The test soil samples were taken from a fresh

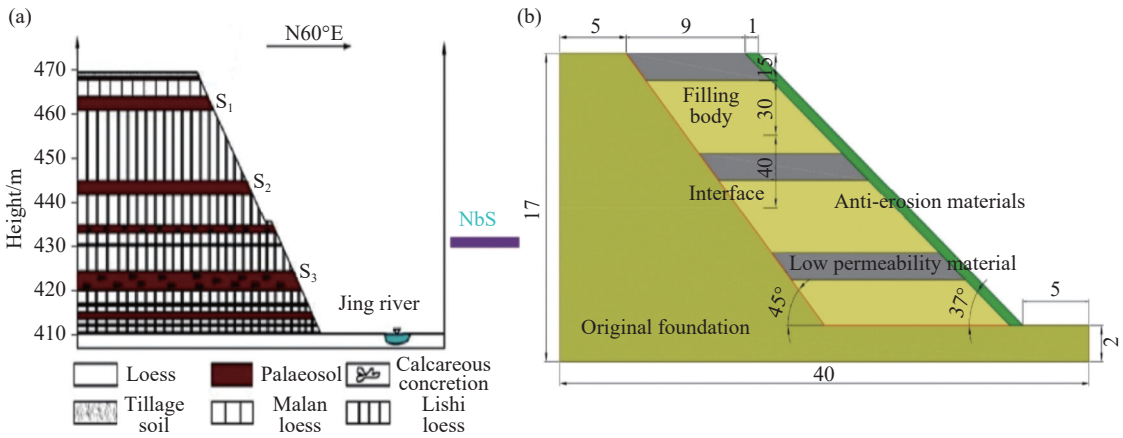

Fig. 4 Water-control structure of loess filling slope based on the NbS concept (a. schematic diagram of the overall slope structure, b. detailed view of the slope water control structure)

section plane in Yan'an and were classified as Malan loess. The soil was loose and wormholes and plant roots were visible (Fig. 5). According to the "Standard for Geotechnical Test Methods" (GBT 50123—2019), laboratory geotechnical tests were carried out on the test soil, and basic physical property parameters were obtained (Table 1). The uniformity coefficient C_u=4.6<5, and the curvature coefficient C_c of the test soil samples = 1.05 is between 1 and 3, indicating that the loess soil samples were silty clay with poor gradation and uniform distribution of particles. Fig. 6 is the particle gradation curve of loess samples.

Fig. 5 Undisturbed soil

2.2 The improved loess

Limestone (the main component is $CaCO_3$) burned to produce quicklime CaO (Eq. 1). When quicklime is mixed into loess, it reacts with water to form slaked lime $Ca(OH)_2$ (Eq. 2), and the reaction is called the ripening process. The lime particles form a colloidal structure of calcium hydroxide, the particles are very fine (particle size of about 1 μm), the specific surface area is very large (10–30 m^2/g), which can fill the large pore space in the loess, so that the soil body is arranged more closely, and the permeability of loess is reduced. Meanwhile, cementation binds the soil particles to improve the stability of the soil. Because of its low price, quicklime can be used to improve loess fill and form a low-permeability layer in slope filling projects. When the dosage of lime is 9%, the permeability of the improved loess is the lowest, and the improvement effect is the most obvious (Gao et al. 2016); therefore, 9% lime is selected to improve the filler of the loess filling slope, thus forming a low-permeability material.

$$CaCO_3 \xlongequal{\text{Baking}} CaO(\text{Quick lime}) + CO_2 \uparrow \quad (1)$$

$$CaO + H_2O \xlongequal{\text{Curing Heat release}} Ca(OH)_2(\text{Slake Lime}) \quad (2)$$

The filler of the loess filling slope is formed by artificial disturbance and remolded loess, changing the original structure of loess. Under the action of rainfall, the surface of the filling slope is prone to erosion failure such as gully formation. The new loess curing agent modified cellulose is made of two kinds of modified cellulose (B and C) and two kinds of inorganic additives (A and D) through crosslinking polymerization, with which the improvement of loess not only solves the problem

Table 1 The basic physical and mechanical parameters of experimental soil samples

Name	Natural moisture content/%	Specific gravity	Sand gravel >0.075 mm/%	Powder particle 0.005–0.075 mm/%	Clay particle <0.005 mm/%	Liquid limit/w_l	Plastic limit/w_p	Plasticity limit index/I_p
Yan'an loess	10.65	2.71	14.89	69.23	15.88	28.84	16.53	12.31

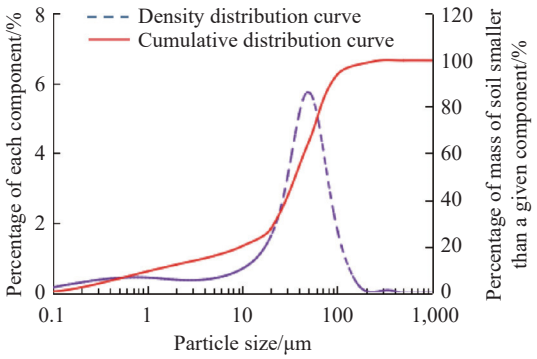

Fig. 6 Particle gradation curve of loess samples

of anti-erosion of slopes, but also has a good ecological effect. Therefore, from the anti-erosion effect, ecological effect, and other factors considered, selecting 0.34% (modified material and soil particles mass ratio) of modified cellulose-improved loess to form an anti-erosion surface layer is very feasible (Ren et al. 2021).

2.3 Long-term performance validation of modified materials

While short-term efficacy is established, long-term validation remains critical for engineering adoption. Lime-modified layers exhibit progressive self-healing: carbonation reactions transform $Ca(OH)_2 \rightarrow CaCO_3$ over 6 months to 24 months, sealing new microcracks (Jiang et al. 2025). Cellulose polymers demonstrate hydrolytic stability: Fourier Transform Infrared Spectroscopy (FTIR) analysis confirms >90% $CONH_2$ group retention after 18-month UV/water exposure, maintaining erosion resistance through covalent cross-linking (Hallstein et al. 2024). Cellulose-modified surfaces achieved 89% native grass coverage within 8 months vs. 37% on bare loess, and DeHydrogenase Activity (DHA) tests show microbial biomass recovery to 95% of natural loess levels after cellulose degradation (≈2 years), and lime stabilization reduces Cd/Pb leaching by 63%–77%, preventing groundwater contamination (Zhou et al. 2025).

2.4 Determination of engineering properties of remolded loess and improved loess

The air-dried loess was crushed and passed through the standard sieve of 2 mm, then the soil samples were mixed with 9% quicklime and 0.34% of modified cellulose for improvement, and the related engineering characteristics of remolded loess and improved loess were measured. The engineering properties of improved loess (Table 2) directly inform the design parameters for physical model construction and numerical simulations. The liquid limit and plastic limit joint determination method shows that the liquid limit, plastic limit and plasticity index of modified cellulose-improved loess are all increased compared with remolded loess, indicating that the improved loess has higher water retention performance. The plasticity index of lime-modified loess is reduced, and hydrophilicity was weakened, which is conducive to the stability of the slope. The maximum dry density and the optimum water content of remolded loess and lime-amended loess were determined by the compaction tests, and the modified cellulose is liquid, so the maximum dry density and optimum water content were chosen to be consistent with those of remolded loess. The calcium oxide in 9% lime-amended loess reacts exothermically with water, consumes part of the water, and expands rapidly in volume, resulting in a decrease in the maximum dry density, and an increase in the optimum water content compared with that of remolded loess. According to the optimum water content, infiltration tests were carried out on three kinds of loess, in which two kinds of improved loess were required to be maintained for 7 days and then tested. The saturated infiltration coefficient of the original loess was 4.36×10^{-6} m/s, and due to the remolded loess disturbing the original structure and increasing the moisture transport path, the infiltration coefficient increased to 8.39×10^{-6} m/s. The infiltration coefficients of

Table 2 Determination of engineering properties of remolded loess and improved loess

Soil sample name	Liquid limit/w_l	Plastic limit/w_p	Plasticity limit index/I_p	Maximum dry density/ g/cm^3	Optimum moisture content/ %	Saturated permeability coefficient K_{sat}/m·s^{-1}	Cohesive force/ kPa	Internal friction angle/°
Remodeled loess	28.84	16.53	12.31	1.73	16	8.39×10^{-6}	17.05	25.32
9% lime-amended loess	33.53	20.19	11.49	1.62	20	9.57×10^{-7}	32.03	26.68
0.34% modified cellulose-improved loess	42.17	23.95	18.22	1.73	20	4.04×10^{-7}	57.10	28.87

the two kinds of improved loess compared to that of the remolded loess were reduced by nearly one order of magnitude, this is due to the reaction of lime-amended loess with water to form calcium hydroxide fine-grained colloids to fill the pore space, and modified cellulose adsorption on the surface of the soil particles to form agglomerates, both of which reduced the pore area and blocked the moisture transport path.

Lime treatment achieved a 95.18% ± 1.2% reduction in saturated permeability (Relative Standard Deviation (RSD) = 1.26%, n = 5), while modified cellulose yielded a permeability of 4.04×10^{-7} m/s ± 0.21×10^{-7} (RSD = 5.2%, n = 5). Shear strength enhancements were equally robust: Lime-amended loess increased cohesion by 87.8% ± 3.5% (32.03 vs. 17.05 kPa), and cellulose treatment boosted it by 234.9% ± 8.2% (57.10 vs. 17.05 kPa, n = 3). Erosion control efficacy was validated through repeated trials, showing a 71.6% ± 3.8% reduction in erosion volume (95% CI: 67.8–75.4%) for slopes with water-control structures compared to untreated slopes.

Compaction degree and water content are the main controlling factors affecting the shear strength of loess, and compaction degree is positively proportional to shear strength and inversely proportional to water content. The cohesive force and internal friction angle of the three soils in Table 2 were measured under the condition of 90% compaction degree and 22% water content. The results show that the cohesive force and internal friction angle of lime-amended and modified cellulose-modified loess increased and the shear strength of lime-amended loess increased the most. Fig. 7 shows the SEM images of the three soils scanned by SEM and magnified 2,000 times. SEM analysis (Fig. 7) reveals that lime modification generates calcium hydroxide colloids, these colloids are marked as "Aggregate" in the figure, presenting as fine flocculent aggregates (Fig. 7b) that occlude macropores (> 5 μm), reducing permeability by 95.18% (Table 2). This pore-filling effect decreases hydraulic pathways, directly explaining the lowered saturated permeability. Conversely, modified cellulose (Fig. 7c) forms polymer bridges via $CONH_2$ groups, bonding soil particles into aggregates. This microstructural bridging enhances cohesive strength by 234.9% (Table 2) by resisting particle dislocation under shear stress.

3 Comparative artificial rainfall physical simulation tests on loess filling slopes with and without water control structures

3.1 Test programs

3.1.1 Test devices

The artificial rainfall physical modeling tests on loess filling slope were carried out on site at the foot of the slope in He Village, Ganguyi Town, Baota District, Yan'an City, which was mainly composed of a model frame, a rainfall system and a data monitoring and collecting system. The size of the model frame is 4.0 × 2.5 × 1.7 m; the main body was made of concrete and masonry red brick with an observation window on one side (Fig. 8), cement mortar was smeared on the inner side and a polyurethane waterproof coating was brushed on it, and the bottom part of the model frame was tamped by a rammer on the site. The artificial rainfall system consists of 28 low-pressure fog nozzles, and the rainfall uniformity can reach 86%, which can meet the test requirements. Fig. 9 is the schematic diagram of the loess filling slope model.

3.1.2 Data monitoring and acquisition system

The data monitoring and acquisition system mainly consists of volumetric water content sensors (model EC-5, Decagon, USA), matrix suction sensors (model MPS-6, Decagon, USA), pore water pressure sensors (model HC-25, made in China), earth pressure sensors (model HC-16,

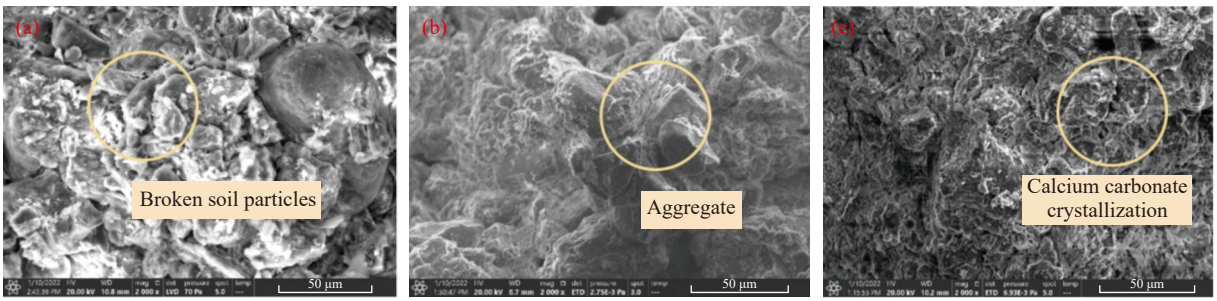

Fig. 7 Microstructure of loess magnified 2000 times (90% compaction degree) (a. the remolded loess, b. lime-amended loess, c. the modified cellulose-improves loess)

Fig. 8 Model frame

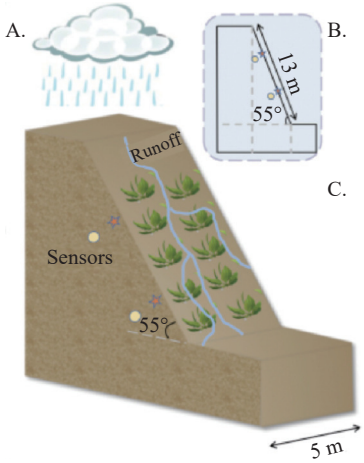

Fig. 9 Schematic diagram of the loess filling slope model

made in China), and three-dimensional laser scanner (model Riegl VZ-400). The sensors were laid out in three layers, with 11 each of matrix suction and water content sensors were placed at $1^{\#}$–$11^{\#}$ measuring point positions, four each of pore water pressure sensors and soil pressure sensors were placed at $1^{\#}$, $3^{\#}$, $7^{\#}$ and $10^{\#}$ measuring point positions respectively, totaling 30 sensors (Fig. 10), and the numbering of the sensors was consistent with the numbering of the measuring point positions.

3.1.3 Similarity ratios

This test was scaled down to 1:20 based on prototype slopes in Yan'an with an average height of 60 m (e.g., Jingyang landslide), mainly to achieve geometric similarity, boundary conditions similarity (similar rainfall conditions and large lateral dimensions to overcome the constraints of boundary conditions), initial conditions similarity (mainly similar compaction degree and initial moisture content) and mechanical properties similarity, so that the artificial rainfall test methods have a certain applicability and feasibility. According to the similarity theorem quantitative analysis method, the similarity constant was n = 20, and the main similarity relations of loess filling slopes were derived (Table 3), in which the slope size (l), soil density (ρ) and gravity acceleration (g) were taken as the basic physical quantities, and the remaining physical quantities were the derived similarity criterion.

3.1.4 Physical model

(1) Model construction

According to the field investigation of the filling slopes in Yan'an area, the landslide of Jiang Liu Driving School in Jingyang South Loess Plateau was used as a test geological prototype. According to the profile of this landslide, it was known that the thickness of the paleosol layer in the area is in the range of 2.5–4 m, and the thickness of the neighboring paleosol layer was in the range of 4–11 m (Nan et al. 2021). Taking this as a reference, the average thickness of the paleosol layer was taken as 3 m, the adjacent thickness was taken as 8 m, and according to the geometrical similarity ratio $C_l = 20$, the thickness of the low-permeability layer and the adjacent layer were determined as 0.15 m and 0.4 m respectively. The gradient was the same as that of the prototype, the dimensions of the filling slope model with water-control struc-

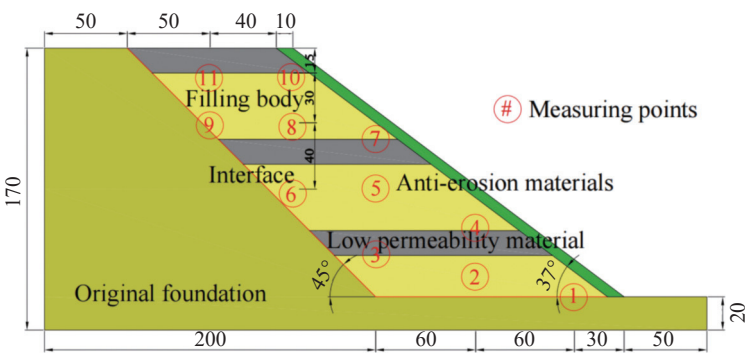

Fig. 10 Profile of the loess filling slope measurement point location layout

Table 3 Main similarity relationships in loess filling slope model

The physical quantity	Notation	Dimension of quantity	Relationship of similarity	Similar constant
Slope dimension (the basic quantity)	l	L	$C_l = n$	n
Soil density (the basic quantity)	ρ	ML^{-3}	$C_\rho = 1$	1
Gravitation acceleration (the basic quantity)	g	LT^{-2}	$C_g = 1$	1
Elastic modulus	E	$ML^{-1}T^{-2}$	$C_E = 1$	1
Poisson's ratio	μ	1	$C_\mu = 1$	1
Stress	σ	$ML^{-1}T^{-2}$	$C_\sigma = C_l C_\rho C_g$	n
Deformation	ε	1	$C_\varepsilon = 1$	1
Pore water pressure	u	$ML^{-1}T^{-2}$	$C_u = C_l C_\rho C_g$	n
Soil cohesive force	c	$ML^{-1}T^{-2}$	$C_c = 1$	1
Internal friction angle	φ	1	$C_\varphi = 1$	1
Permeability coefficient	k	LT^{-1}	$C_k = 1$	1
Moisture content	w	1	$C_w = 1$	1
Displacement	d	L	$C_d = n$	n
Rainfall intensity	q	LT^{-1}	$C_q = \sqrt{C_l}\sqrt{C_g}$	$\sqrt{n}$
Time	t	T	$C_t = \frac{\sqrt{C_l}}{\sqrt{C_g}}$	$\sqrt{n}$

ture referred to Fig. 10, as marked therein, and the dimensions of the filling slope without water-control structure were the same as those of the water-control structure, and filler was pure loess.

The test materials were the soil around the test site, which were sieved with 2 cm aperture and then evenly spread out for turning and crushing. Slope filling was used in layered compacting method, the original slope was filled according to the compaction degree of 100%, the filling slope was filled according to the compaction degree of 90%, and the moisture content was configured according to the optimal moisture content of ±2%. Each layer of soil was sampled using a ring knife and its density was measured until the test requirements were met (Eq. 3). Sensors were buried and calibrated, and the slope was cut according to a 37° slope angle after the loess filling slopes were filled. Then the plastic film was spread on the surface of the slope to reduce the evaporation of water from the slope, and after 24 h of resting, the rainfall tests were started.

$$\rho = \rho_{\max} \cdot \lambda \cdot \left(1 + w_{op}\right) \tag{3}$$

In the formula, $\rho_{\max}$ (g/cm^3) is the maximum dry density, w_{op} is the optimum moisture content, and λ is the compaction degree.

(2) Rainfall condition

According to the meteorological department of Yan'an, the maximum rainfall of 1 h in this area was 62 mm, according to the similarity ratio of rainfall intensity Eq. 4:

$$C_q = C_l^{1/2} \cdot C_g^{1/2} \tag{4}$$

In the formula, C_q was the rainfall intensity similarity ratio, C_l was the geometric similarity ratio, C_g was the gravity similarity ratio, taken as 1. It could be determined that $C_q = 4.47$, and thus the rainfall intensity of the model tests was 13.87 mm/h. According to the meteorological department classification, it was classified as extraordinarily heavy rainfall level. The uniform type of rainfall was used to carry out two groups of artificial rainfall tests on filling slopes with or without water-control structures, until the deformation and destruction of filling slopes stopped after no obvious changes in deformation.

3.2 Analysis of test results

3.2.1 Instability mode of loess filling slope under rainfall action

Fig. 11 and Fig. 12 show the damage process of the slope surface without and with a water- control structure and the 3D deformation pattern generated by Surfer software from the point cloud data collected by a 3D laser scanner, respectively. The filling slope without a water-control structure, due to the inherent water sensitivity and structural nature of loess, exhibited rapid dispersion under the erosive effect of rainfall and was characterized by fluidization to the fore-edge of the slope, with a long sliding distance and a large accumulation range. The loess filling slope with a water-control

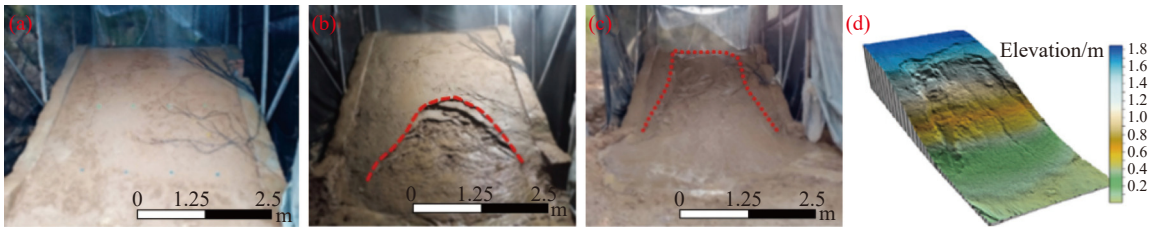

Fig. 11 Failure mode of slope surface without a water-control structure (a. rainfall beginning on 2024.8.13 at 13:00, b. rainfall duration on 2024.8.16 at 2:12, c. rainfall ending on 2024.8.16 at 17:46, d. three-dimensional deformation model diagram)

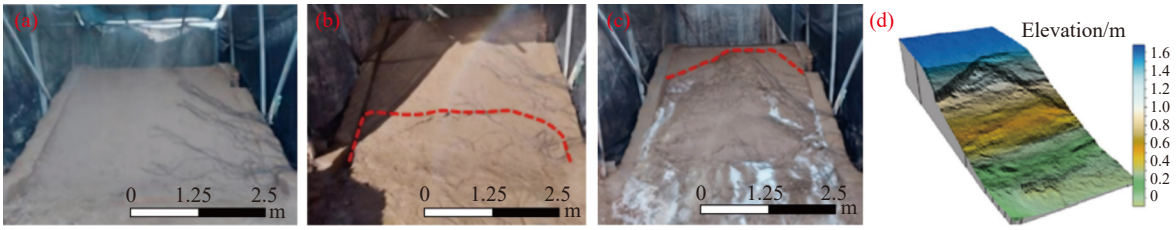

Fig. 12 Failure mode of slope with a water-control structure (a. rainfall beginning on 2024.8.23 at 10:00, b. rainfall duration on 2024.8.25 at 08:35, c. rainfall ending on 2024.8.29 at 9:00, d. three-dimensional deformation model diagram)

structure was more intact during the rainfall process because the erosion-resistant surface layer played the role of a crust, and the top of the slope did not undergo large deformation damage after the end of the rainfall, and the rainfall duration was longer than that of the slope without a water-control structure.

The destabilization modes of loess slope without a water-control structure are as follows: rainfall infiltration, filling-interface cracks generation, local landslide at the fore-edge of the slope, development and expansion of tension cracks at the slope crest, landslide damage in the middle and upper parts of the slope, collapse of the slope shoulder, penetration of the sliding surface, and final skidding failure, which showed the characteristics of the slide collapse and long-distance flow-slip, and the damage mode was the sudden collapse and flow slide destruction.

The destabilization mode of the loess slope with a water-controlled structure was: Rainfall infiltration, collapse damage at the fore-edge of the slope, crack generation on the slope crest and surface, slip damage in the middle part of the slope, localized destabilization in the upper part, and collapse at the slope shoulder, which showed the characteristics of intact slide body and short-distance shear slip, and the destabilizing mode was gradual shear-slip destabilization.

According to the accurate calculation of the three laser scanning point cloud data, the erosion volume of the slope without a water-control structure was as high as 0.9372 m^3 at the end of rainfall, and the erosion volume of the slope with a water control structure was obviously reduced at the same time compared with the slope without a water-control structure, and the erosion volume was only 0.2665 m^3 at the end of rainfall.

3.2.2 Analysis of the test data results

As the rainfall continued, the wetting peak gradually moved down, and the Moisture Content sensors (MC) started to respond to the rainfall one after another. For slopes without a water-control structure, Fig. 13 showed the water content change curves with time at the main measurement points. The sensors responded more quickly and simultaneously, reflecting rapid and uniform infiltration that led to overall instability.

In contrast, for slopes with a water-control structure, Fig. 14 showed the water content change curves with time at the main measurement points. The MC-11 sensor at the top of the slope responded first at 683 min, indicating the arrival of the wetting front, with a water content of 19.2% at the time of response. As water continued to infiltrate, MC-1, MC-3, and MC-7 began to respond in turn at 1,041 min, 1,169 min, and 1,639 min, respectively. Compared with the slopes without a water-control structure, the response time of each sensor increased significantly, demonstrating that the low-permeability layers effectively retarded the rate of water transport and act as a barrier to rainfall. The sequential response of deeper positions further highlights this retarding effect. A peak

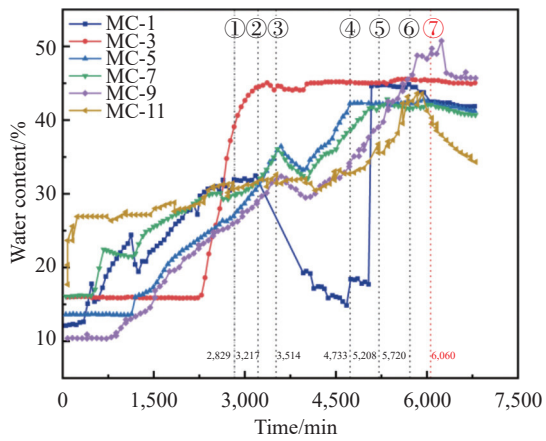

Fig. 13 Curve of water content with time at the main measurement points of slopes without water-control structure

Notes: ① Microcrack development at the interface; ② interface cracks continue to expand; ③ local collapse of the slope foot; ④ slope shoulder crack development; ⑤ localized collapse in the middle of the slope and crack developement at the top of the slope; ⑥ slope shoulder began to collapse; ⑦ rainfall stopped

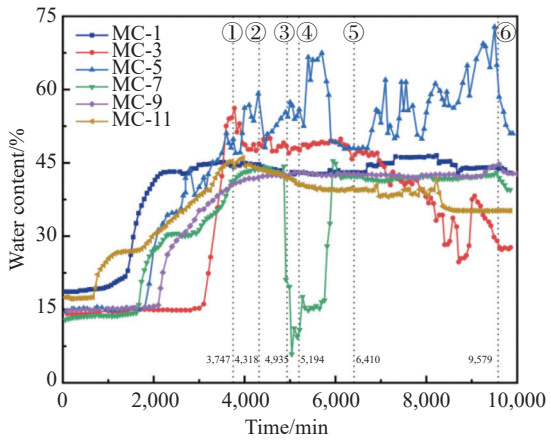

Fig. 14 Curve of water content with time at the main measurement points of slopes with water-control structure

Notes: ① Slope toe slid overall; ② the back wall of the landslide saturated by rainfall; ③ the second sliding and slope top tension crack development; ④ the third sliding; ⑤ slope shoulder collapsed; ⑥ rainfall stopped

water content of 59.4% measured by MC-3 corresponds to the local saturation and softening of the soil preceding slope failure.

The loess filling slope was artificially compacted and belongs to typical unsaturated loess, in which there was a fourth phase composed of a water-gas interface (shrinkage film) in addition to the three phases of soil particles, pore water and pore gas. The theory of shear strength of unsaturated soils proposed by Fredlund et al. showed that the pore water pressure is less than the pore gas pressure, and the pressure difference between the two is the matrix suction, which contributes to the shear strength of the soil body (Fredlund et al. 1978). The trend of matrix suction change with and without a water-control structure was similar (Fig. 15 and Fig. 16); rainfall predominantly infiltrated in the early stage, and after the matrix suction sensors (MS) responded to the rainfall, it rapidly declined from a stationary phase. The unsaturated soil became saturated after rainfall continued infiltration, and the rate of decline of matrix suction began to slow down and eventually stabilized. Compared with the slopes without a water-control structure, the response times of matrix suction sensors of loess slopes with a water-control structure were delayed, and the most significant difference was observed in the sensor located

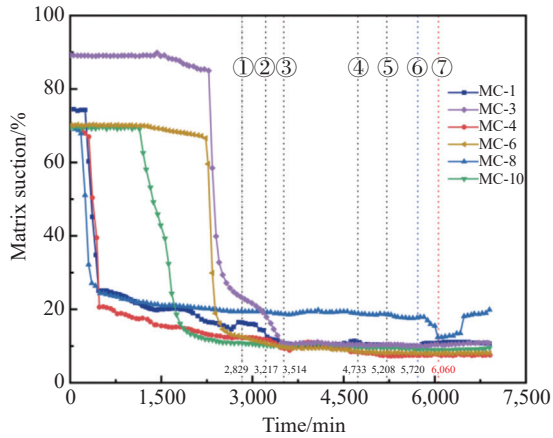

Fig. 15 Matrix suction curves with time at the main measurement points of slopes without water-control structure (①-⑦ are slope destruction stages, consistent with Fig. 13)

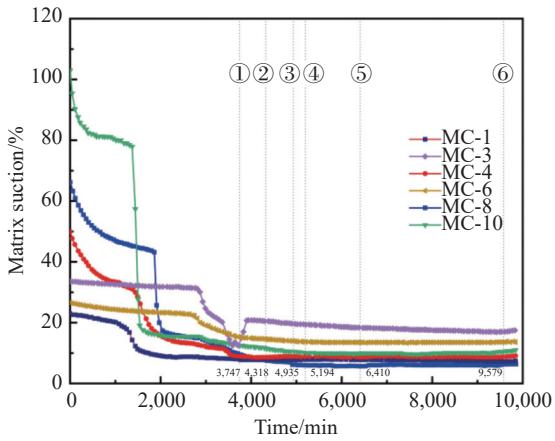

Fig. 16 Matrix suction curves with time at the main measurement points of slopes with water-control structure (①-⑥ are slope destruction stages, consistent with Fig. 14)

at the top of the slope, which once again indicated that the existence of the low-permeability layer effectively slowed water transport and explained the shift from fluidized collapse (Fig. 13) to gradual shear-slip (Fig. 14).

The Pore Water Pressure sensors (PWP) were placed at the 1#, 3#, 7# and 10# measuring points, and the PWP-10 sensor was damaged and the collected data were invalid. The slope without a water-control structure (Fig. 17), when cracks were generated within the slope, experienced rapid recharged along the cracks and the pore water pressure rose rapidly. However, as the slope underwent deformation and damage, the cracks continued to expand, and the rainwater continued to seep and drain along the cracks, resulting in a rapid decrease in pore water pressure.

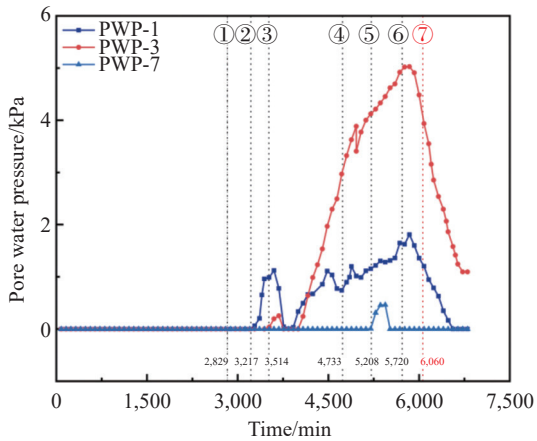

Fig. 17 Pore water pressure curves with time at the main measurement points of slopes without water-control structure (①-⑦ are slope destruction stages, consistent with Fig. 13)

The change rule of pore water pressure of the slope with a water-control structure was completely different from that of the slope without a water-control structure, and the change rule of pore water pressure of the slope with water-control structure was completely different (Fig. 18). The most obvious difference was that the pore water pressure had only one wave peak, and it could be maintained for a period of time without large fluctuation, which means that the water did not infiltrate rapidly and the low-permeability layer had an obvious water-isolating effect.

The buried depth of earth pressure sensor EP-3 was in the deepest part of the slope body. In the slope without a water-control structure, the local collapse in a small range did not cause changes in earth pressure at the measuring point, but it started to rise sharply when the rainfall lasted 4,685 min, and the earth pressure reached 5.53 kPa at 4,733

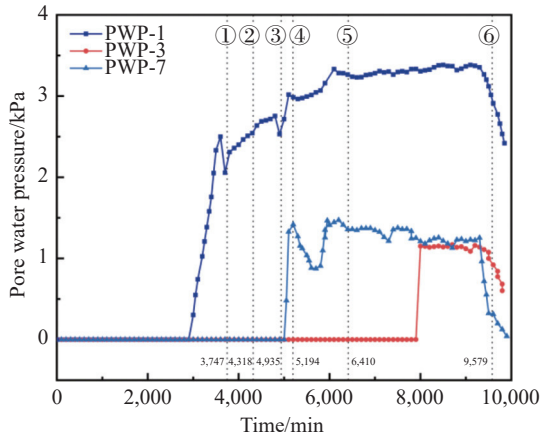

Fig. 18 Pore water pressure curves with time at the main measurement points of slopes with water-control structure (①-⑥ are slope destruction stages, consistent with Fig. 14)

min. On a macro level, the slope showed local collapse in the middle of the slope. The sliding range was large, and the sliding surface was deep, which caused the earth pressure to increase rapidly. The earth pressure reached its peak value in 5, 208 min, up to 7.41 kPa (Fig. 19). In the slope with a water-controlled structure, the variation trend of earth pressure was consistent with the deformation and failure stages of the slope, and the EP-3 sensor did not respond. This was due to the arrangement of three low-permeability layers, which prevented the influence depth of the sliding body from reaching the monitoring depth of measuring point 3# (Fig. 20).

Field experiment monitoring data (Figs. 13–20) validate the mechanical mechanisms proposed in Section 4. For instance, the delayed matric suction response (Fig. 16) and reduced pore water pres-

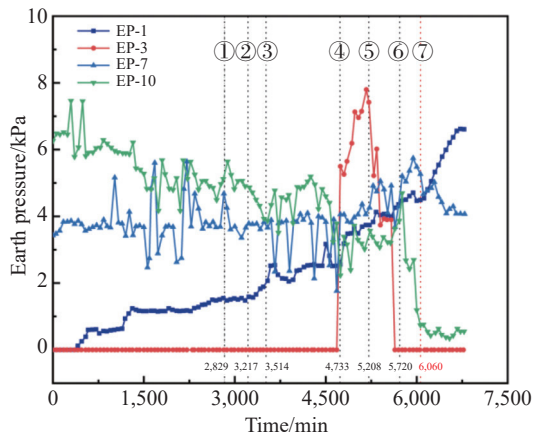

Fig. 19 Earth pressure curves with time at the main measurement points of slopes without water-control structure (①-⑦ are slope destruction stages, consistent with Fig. 13)

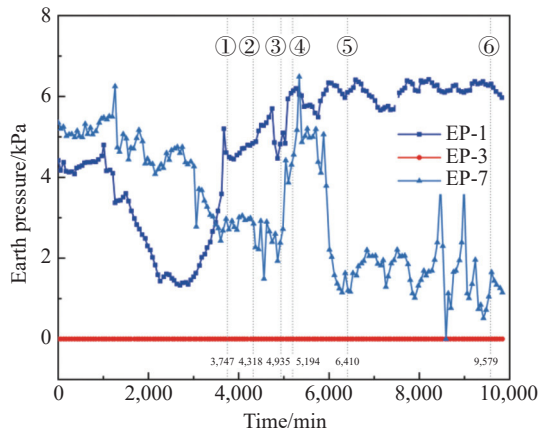

Fig. 20 Earth pressure curves with time at the main measurement points of slopes with water-control structure (①-⑥ are slope destruction stages, consistent with Fig. 14)

sure fluctuations (Fig. 18) in slopes with a water-control structures align with the shear-strength theory for unsaturated soils (Fredlund et al. 1978). These experimental results are critical for calibrating the seepage-stress-deformation coupling in subsequent numerical simulations.

4 Mechanical mechanism analysis of loess filling slope stability

Morgenster-Price is a rigid-body limit method widely accepted by engineering geology. It is assumed that the sliding surface can be of any shape, and this method still satisfies the balance of torque and force. The Morgenstern-Price method (Fig. 21) provides the theoretical framework for stability calculations in numerical simulations. Its force/moment equilibrium equations govern slope failure criteria in Geo-Studio's SLOPE/W module, enabling direct comparison between physical model failures (Section 3.2.1) and simulated stability coefficients (Section 5). The solution process of this method is as follows: the equilibrium differential equation of torque and force on the sliding surface of an arbitrary curve is established, and the stability coefficient is obtained according to the boundary conditions of the slope and the assumed functional relationship. Fig. 21 is the stress analysis diagram of the Morgenster-Price method.

(1) Theoretical mechanical modeling of slope

First, for the differential slice shown in Fig. 21, a moment balance equation located at the bottom midpoint is established, then:

$$E'\left[(y-y')-\left(-\frac{dy}{2}\right)\right]-(E'+dE')\left[(y+dy)-(y_i'+dy_i')+\left(-\frac{dy}{2}\right)\right]-\frac{Xdy}{2}-(X+dX)\frac{dx}{2}+U\left[(y-h)-\left(-\frac{dy}{2}\right)\right]-(U+dU)\left[(y+dy)-(h-dh)+\left(-\frac{dy}{2}\right)\right]-dU_s.g=0 \quad (5)$$

The formula (5) is simplified to:

$$X=\frac{d}{dx}(E'y_i')-y\frac{dE'}{dx}+\frac{d}{dx}(Uh)-y\frac{dU}{dx} \quad (6)$$

In the second step, the equilibrium equation for the force in the direction normal to the bottom of the differential slice is established as:

$$dN'+dU_s=dW\cos\alpha-dX\cos\alpha-dE'\sin\alpha-dU\sin\alpha \quad (7)$$

Similarly, the force balance equation in the tangential direction at the bottom of the bar is established, then:

$$dT=dE'\cos\alpha+dUcso\alpha-dX\sin\alpha+dW\sin\alpha \quad (8)$$

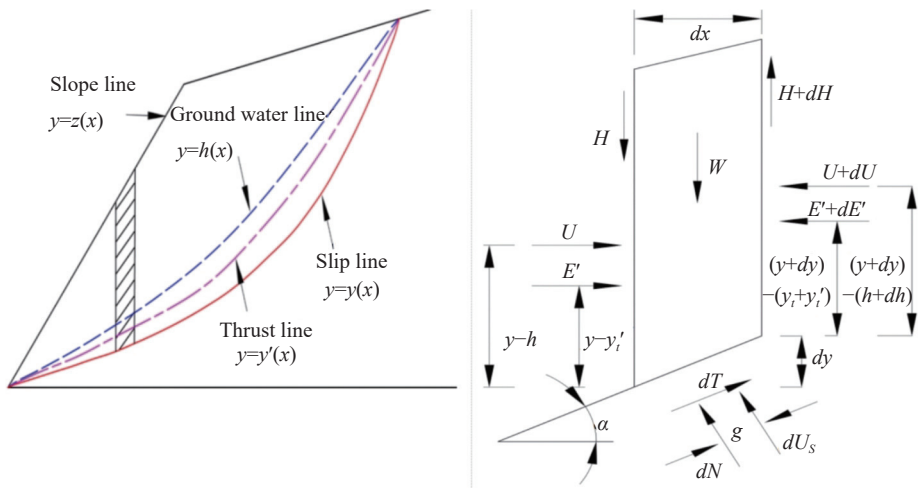

Fig. 21 Stress analysis diagram of the Morgenster-Price method

If the Mohr-Coulomb criterion is represented by a differential, then there is:

$$dT = \frac{1}{F_{st}}\left(\frac{c'dx}{\cos\alpha} + ddN'\tan\varphi'\right) \quad (9)$$

In order to facilitate the calculation and simplify the physical quantities in the formula, the effective normal stress E' and the lateral pore water pressure U are expressed as the total normal stress E, then: $E = E' + U$. According to the previous hypothesis, the functional relationship between the normal stress E and the tangential stress X on both sides of the strip is: $X = \lambda f(x)E$. Therefore, the above equations are simplified and then merged into:

$$X = \frac{d}{dx}Ey - y\frac{dE}{dx} \quad (10)$$

$$(Kx + L)\frac{dE}{dx} + KE = Nx + p \quad (11)$$

And for the integral of $x_i \to x_{i+1}$ (Eq. 11), the result is:

$$E_{i+1} = \frac{1}{L + K\triangle x}(E_i L) + \frac{N\triangle x^2}{2} + p\triangle x \quad (12)$$

(2) Slope stability coefficient solution

The limit equilibrium of the overall slope requires that the last strip of this slope body satisfies: $E_n = 0$. Then the moments on both sides of the strip can be found by the differential equation (Eq. 10):

$$M_{i+1} = E_{i+1}(y - y_i)_{i+1} = \int_x^{x+1}\left(X - E\frac{dy}{dx}\right)dx \quad (13)$$

And the torque needs to be satisfy:

$$M_n = \int_{x_0}^{x}\left(X - E\frac{dy}{dx}\right)dx = 0 \quad (14)$$

The method is iterated several times to find the λ (arbitrarily chosen as a constant) that satisfies all equilibrium equations and F_s. The first step is to assume an initial value of λ and F_s, then integrate through each strip one by one, and finally check if E_n and M_n are zero. If they are not zero, then iterations need to be continued until the desired accuracy is achieved, at which point F_s is the slope stability coefficient.

5 Discussion

The characteristics of the low-permeability layer (number of layers, thickness, dip angle) have an important influence on the seepage regulation of loess filling slopes, and the following discussion analyses can provide more feasible technical support for the development of filling projects.

5.1 Influence of the number of low-permeability layers on the seepage field of loess filling slopes

The Morgenster-Price method of the SLOPE/W module in GeoStudio was used to calculate the influence of different number of low-permeability layers on the seepage field of the loess filling slope. The model size is shown in Fig. 8. Material properties (permeability, strength from Section 2.3) define the parameters of soil layers, physical test data (infiltration rates, failure modes from Section 3) calibrate rainfall-seepage boundaries and mechanical analysis (Section 4) sets stability computation models. The groundwater in the loess area is deeply buried, so the bottom boundary of the model can be set as the zero pore pressure boundary, the two sides of the model can be set as the undrained boundary, and the slope top can be set as the rainfall infiltration boundary. The rainfall intensity is 50 mm/d and the rainfall boundary on the slope should be reduced to 39.9 mm/d according to the slope of 37°.

Fig. 22 shows the distribution of transient seepage volume water content of loess filling slope after 10 d steady seepage under four different working conditions. The infiltration line of the loess slope without low-permeability layer was arc-shaped (Fig. 22a), while the infiltration line of the loess slope with low-permeability layer had an obvious inflection point (Fig. 22b-22d). With continuous rainfall, the effect of the low-permeability layer on slowing down rainfall infiltration was gradually manifested, and the infiltration line under the low-permeability layer was "concave", especially the first low-permeability layer. The infiltration depth of the slope and wet area with a low-permeability layer decreased significantly compared with that without a low-permeability layer: the maximum infiltration depth of the slope without low-permeability layer reached 4.5 m at the top of the slope, while the infiltration depth of the slope with a low-permeability layer was 1.6 m at the top of the slope, which was 2.9 m lower than that of the slope without a low-permeability layer.

By comparing Fig. 23a (pure loess slope) with Fig. 23b, 23c and 23d (slopes with low-permeability layers), it can be found that the water content of layers 1, 2 and 3 with low-permeability layers changed almost consistently over time, and the influence depth of rainfall did not exceed 3 m. At the monitoring points above 3 m, the water content first increased sharply, then slowed down with the continuous rainfall, and finally became stable. The

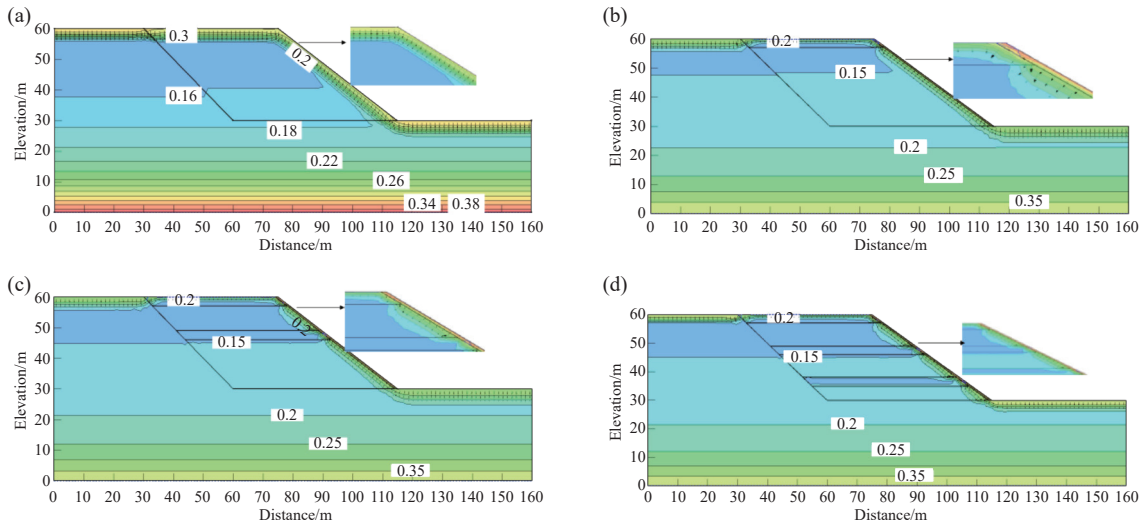

Fig. 22 Transient distribution diagram of volumetric moisture content of the loess filling slope at 10 d rainfall (a. pure loess filling slope without a low-permeability layer, b. the loess filling slope with one low-permeability layer, c. the loess filling slope with two low-permeability layers, d. the loess filling slope with three low-permeability layers)

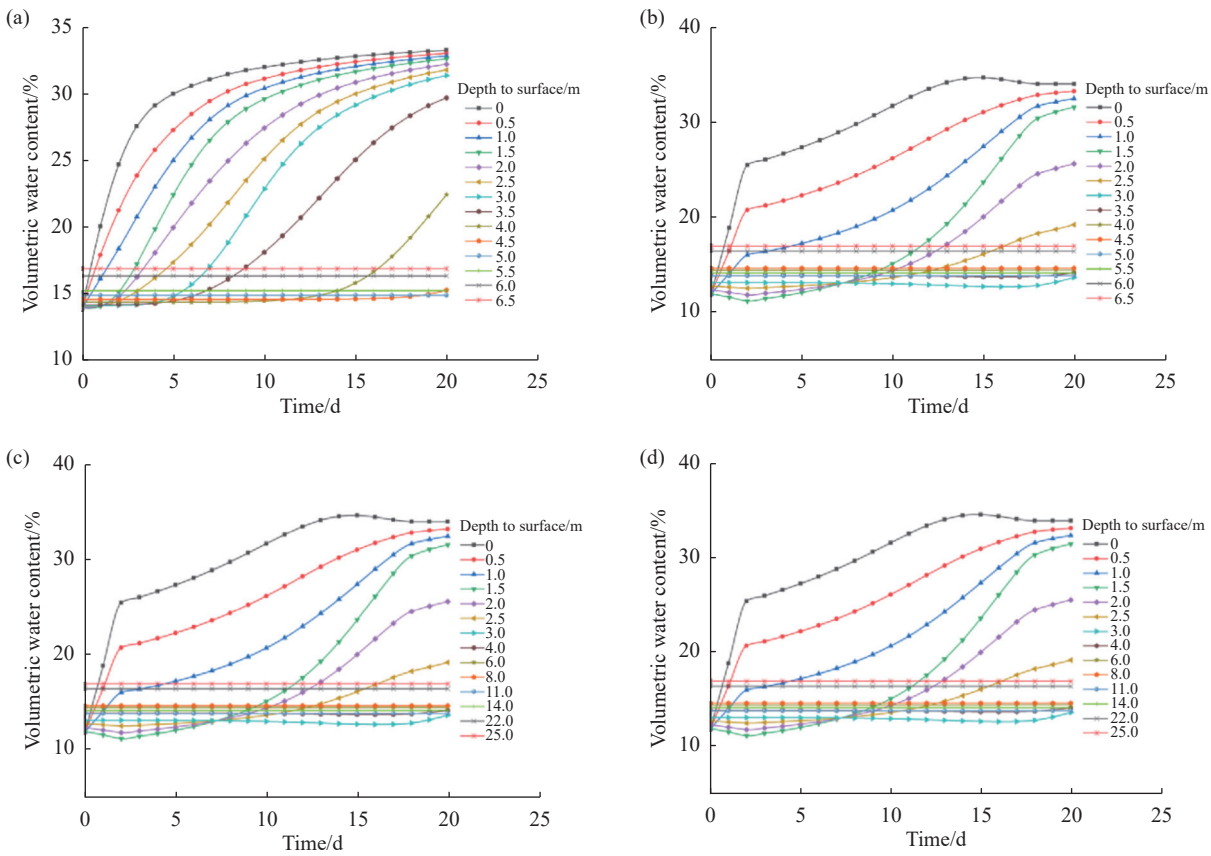

Fig. 23 Variation curve of moisture content of the monitoring line of the loess filling slope with rainfall time (a. pure loess filling slope without a low-permeability layer, b. the loess filling slope with one low-permeability layer, c. the loess filling slope with two low-permeability layers, d. the loess filling slope with three low-permeability layers)

effect of two or three layers of low-permeability on the seepage field of the loess filling slope was not great; the insignificant impact of additional low-permeability layers on seepage control stems from the saturation threshold effect, where the uppermost layer (optimized at 3 m thickness and 2° dip

angle) dominates infiltration resistance by forming a capillary barrier upon saturation, while deeper layers remain hydraulically inactive due to permeability contrasts (>95% reduction via lime modification) and insufficient hydraulic head to activate secondary barriers.

The maximum moisture content of the slope with non-erosive material at the top test point 1 was 32.7%, while that of the slope with an erosion-resistant surface was 49.0%, an increase of 16.3%. The moisture content of the slope with an erosion-resistant surface was not much different at the lower test point, indicating that the erosion-resistant surface has a good water-holding effect, which is conducive to the growth of slope surface plants, but has little influence on the interior of the slope, and reduces the water enrichment in the slope.

5.2 Influence of low-permeability layer thickness on the stability of loess filling slopes

In order to study the influence of the thickness of the low-permeability layer on the seepage and stability of loess filling slopes, three kinds of working conditions with the thickness of the low-permeability layer of 1.5 m, 3 m and 4.5 m were set up to be analyzed in the case of a rainfall intensity of 50 mm/d and rainfall duration of 20 d. As can be seen from Fig. 24, when the thickness of the low-permeability layer was 1.5 m, the maximum infiltration depth of the rainfall slope reached 4.0 m (Fig. 24a), and when the low-permeability layer was 3.0 m and 4.5 m, the depth of influence was almost the same, all within the range of 2.5–3.0 m (Fig. 24b-24c). It is more economical and appropriate to set the thickness of the low-permeability layer of 3.0 m in the loess filling slope.

Fig. 25 shows the relationship between the thickness of the low-permeability layer and the stability of the loess filling slope under the condition of rainfall infiltration. Before the rainfall, the slope stability coefficients of the low-permeability layer thickness of 1.5 m, 3.0 m and 4.5 m were 2.30, 2.33 and 2.37, respectively, and the stability coefficient was positively correlated with the thickness of the low-permeability layer. With the continuous rainfall, the stability coefficient of the slope decreased. By the end of the rainfall, the corresponding stability coefficients dropped to 2.18, 2.22, and 2.27, respectively, by 5.2%, 4.7%, and 4.2%.

5.3 Influence of low-permeability dip angle on stability of loess filling slope

In the field model test and numerical simulation analysis, the horizontal low-permeability layer can slow down the infiltration of rainwater, but there is also the case that rainwater cannot be discharged from the slope body and collects inside the slope body, forming transient retention water. A certain dip angle of the low-permeability layer can allow rainwater to be discharged smoothly, but an excessively large dip angle may reduce the stability of the slope and form a sliding surface. The low-permeability layer was set as one layer, the thickness was 3 m, and the dip angle was 0°, 2° and 4°, respectively, for seepage analysis and stability calculation under three working conditions.

When the dip angle of the low-permeability layer was 0°, the vector cloud at the top of the slope was dominated by vertical infiltration (Fig. 26a), when the low-permeability layer had a certain dip angle, the vector cloud at the top of the slope pointed to the outside of the slope, as shown in Fig. 26b and Fig. 26c. Fig. 27 shows the influence of low seepage layer dip angle on the stabil-

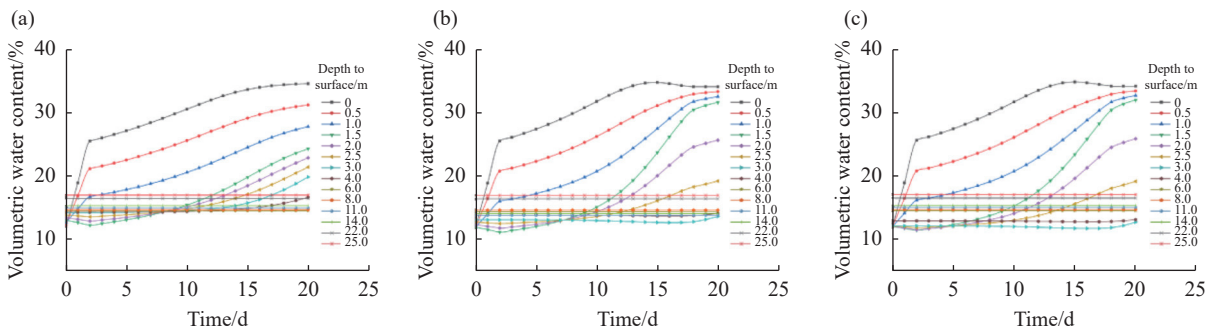

Fig. 24 The variation curve of moisture content of the loess filling slope with rainfall time (a. the thickness of the low-permeability layer was 1.5 m, b. the thickness of the low-permeability layer was 3.0 m, c. the thickness of the low-permeability layer was 4.5 m)

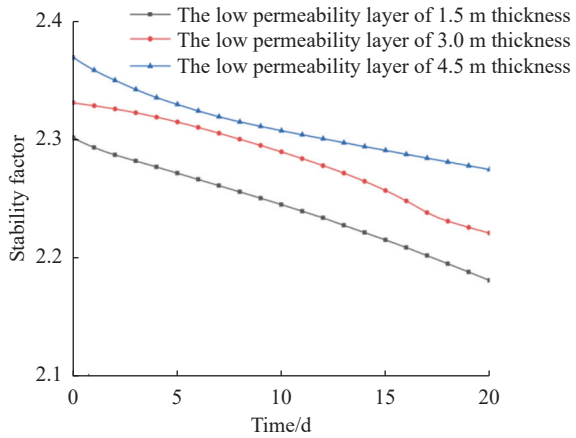

Fig. 25 Effect of low-permeability layer thickness on the stability of the loess filling slope

ity of loess filling slope. Before the rainfall, the stability coefficients of the three working conditions were 2.34, 2.37 and 2.43, respectively. With the end of the rainfall, the stability of the slope with 0° dip angle of the low-permeability layer decreased to 2.22, and the stability coefficients of the slopes with 2° and 4° dip angle decreased to 2.22 and 2.20, respectively, and the slope with 2° showed no change compared with that with 0° dip angle, while the slope with 4° dip angle was reduced by 0.9%.

In the early stage of rainfall, the dip angle of the low-permeability layer was conducive to slope drainage, and in the later stage of rainfall, rainwater accumulated and formed transient retention water at the interface of the loess and low-permeability layer, softening the soil and reducing the shear strength. Therefore, it is more appropriate to choose a 2° dip angle of low-permeability layer of filling projects.

Numerical simulations further confirmed the stability of the loess fill slope, with optimal configurations exhibiting minimal variability: A 3 m-thick, 2°-inclined low-permeability layer maintained stability coefficients of 2.22 ± 0.04 (RSD = 1.8%), outperforming suboptimal designs (e.g., 4.5 m thickness: RSD = 2.6%). All critical results-permeability, shear strength, erosion volume, and stability coefficients-showed statistically significant differences ($p < 0.05$, ANOVA) between control and water-control structures, with variability attributed to soil heterogeneity (±5%), sensor drift (±5%), and image segmentation thresholds (±3%). This rigorous error analysis underscores the solution's field reliability.

According to the characteristics of the loess-paleosoil layered self-stable structure and the concept of NbS, this study proposed the water-controlling structure of loess filling slope: The loess in the filling slope is improved by lime, and the soil on the slope surface is improved by eco-friendly and degradable modified cellulose. In the discussion section, a feasible technical scheme was proposed for the layer number, thickness and dip angle of the low-permeability layer. Compared with existing studies, the stability of loess-paleosol interlayers was not affected by rainfall when the slope angle was 1.5°–5° (average value: 3.2°) (Leng et al. 2017), which was consistent with the 2° engineering layer in this study. Reducing the dip angle to 2° compensates for the heterogeneity problem caused during the compaction process of the fill slope. Peng et al. recorded the local shear of the slope with an interface angle >3° in Tianshui and loess due to water accumulation (Peng et al. 2015). The dip angle of the fill slope was set at 2° within the critical threshold, indicating that the slope setting was reasonable. Yang et al. obtained that the optimal drainage angle of the reinforced slope was 1°–4° by using the numerical simulation method (Yang et al. 2018). However, the model ignored the unique collapsibility of loess, and the physical simulation experiments in this study took into account the seepage characteristics of loess.

After the filling projects are started, the slope surface can be supplemented with turf transplanta-

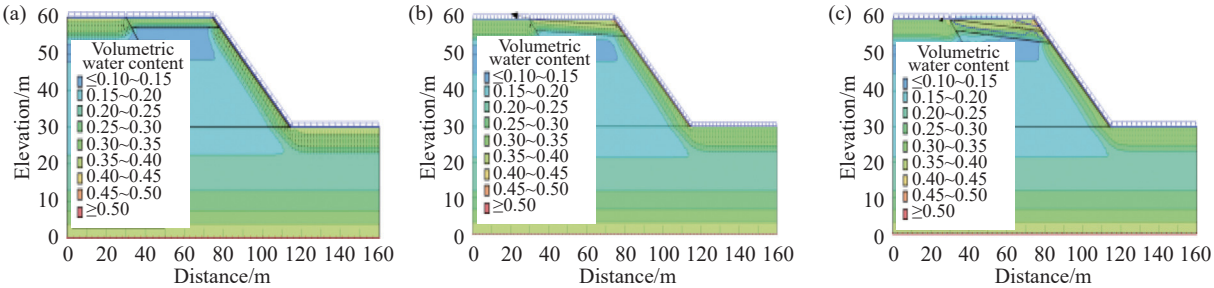

Fig. 26 Effect of low-permeability dip angle on the stability of loess filling slope (a. the dip angle of the low-permeability layer was 0°, b. the dip angle of the low-permeability layer was 2°, c. the dip angle of the low-permeability layer was 4°)

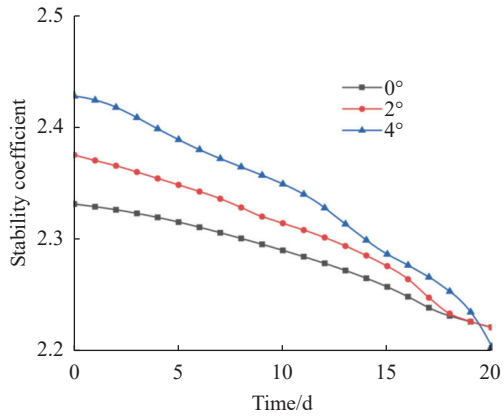

Fig. 27 Effect of low-permeability dip angle on the stability of loess filling slope

tion, seeding of leguminous herbs (alfalfa) and shrubs, and the comprehensive benefits of ecological, economic and social integration can be achieved. In the study, the field modeling experiments were carried out, and the large temperature difference between day and night in the local area had a certain impact on the experimental results, and the influence of significant diurnal temperature variation (up to 15–20°C in Yan'an area) on rainfall infiltration and deformation damage of slopes should be taken into account in subsequent research. This could be achieved by incorporating temperature sensors in physical model tests or adding a temperature field module in numerical simulations to enable thermo-hydro-mechanical coupling analysis. In addition, according to the numerical simulation results, the feasible setup scheme (number of layers, thickness, dip angle, etc.) for the low-permeability layer within the slope is proposed, but the erosion-resistant characteristics of the erosion-resistant surface layer under different working conditions (rainfall intensity, thickness, slope degree) were not considered in this paper and can be further carried out in follow-up studies. While the model experiments demonstrated significant improvements in slope stability through NbS-based water-control structures, this study explicitly acknowledges the exclusion of diurnal temperature fluctuations, which may accelerate crack formation and wet-dry cycling in loess slopes, thereby potentially underestimating real deterioration rates. Future work should integrate thermo-hydro-mechanical coupling to address this limitation.

6 Conclusions

According to the characteristics of the loess-paleosoil layered self-stable structure, and based on the concept of NbS, the water-controlled structure of the loess filling slope was proposed: Lime-improved loess forms a low-permeability layer with high strength similar to the paleosoil layer in the slope, and modified cellulose-improved loess forms an erosion-resistant surface layer on the slope surface. This paper mainly draws the following conclusions:

(1) This study proposes a dual water-control mechanism integrating surface soil stabilization with internal anti-seepage. Both lime-modified materials and cellulose-modified materials significantly enhanced soil strength and reduced permeability. Microscopic mechanism analysis revealed that the calcium hydroxide gel produced by the lime reaction filled the large pores (>5 μm), reducing the saturated permeability coefficient by 95.18%; the modified cellulose, through polymer cross-linking, aggregated the soil particles into clumps, significantly increasing the cohesion by 234.9%.

(2) The artificial rainfall model test showed that compared with the slope without a control structure, the installation of a waterproof structure effectively delayed rainfall infiltration, lasting up to 1,565 min, reducing the erosion by 71.6%, and transforming the failure mode from fluidized collapse to progressive shear failure.

(3) Numerical simulations balanced the trade-off between the drainage benefits of an inclined low-permeability layer and the stability risks associated with excessive dip. The results indicate that a 3 m-thick layer with a 2° dip angle constitutes the optimal configuration, effectively retarding rainfall infiltration while maintaining structural integrity.

Acknowledgements

This study was supported by Key R&D Program Project of Xinjiang Autonomous Region - Key Technologies for Ecological and Geological Environment Restoration of Mines and Green Low Carbon Comprehen - Sive Reuse of Iron Ore Tailings (2023B03011-3); Key Research and Development Project of Xizang Autonomous Region - Research and Application Demonstration of Ecological Restoration Technology for Ecological Sensitive Area Project of Xizang Section of Sichuan Tibet Railway (XZ202401ZY0091). Tianfu Yongxing Laboratory Organized Research Project Funding (2023KJGG05); the National Key Research and Development Program of China (2023YFC3007103).

References

Bao H, Liu C, Lan H, et al. 2022. Time-dependency deterioration of polypropylene fiber reinforced soil and guar gum mixed soil in loess cut-slope protecting. Engineering Geology, 311: 106895. DOI：10.1016/j.enggeo.2022.106895.

Bauduceau N, Berry P, Cecchi C, et al. 2015. Towards an EU research and innovation policy agenda for nature-based solutions & re-naturing cities. Final report of the Horizon 2020 expert group on nature-based solutions and re-naturing cities. Brussels: 1–70. DOI：10.2777/765301.

Chen H, Lee CF, Law KT. 2004. Causative mechanisms of rainfall-induced fill slope failures. Journal of Geotechnical and Geoenvironmental Engineering, 130: 593–602.

Chen Y, Li P, Wang Y, et al. 2024. Unraveling the mystery of water-induced loess disintegration: A comprehensive review of experimental research. Sustainability, 16(6): 2463. DOI：10.3390/su16062463.

Cheng H, Xu R, Wang GL, et al. 2023. Study on the stability of loess high fill slope in Yan'an New Area. Coal Geology of China, 35(10): 52–57. (in Chinese) DOI：10.3969/j.issn.1674-1803.2023.10.09.

Derbyshire E, Dijkstra TA, Smalley IJ, et al. 1994. Failure mechanisms in loess and the effects of moisture content changes on remoulded strength. Quaternary International, 24: 5–15. DOI：10.1016/1040-6182(94)90032-9.

Fredlund DG, Morgenstern NR, Widger RA. 1978. The shear strength of unsaturated soils. Canadian Geotechnical Journal, 15: 313–321. DOI：10.1139/t78-029.

Gabet EJ, Mudd SM. 2006. The mobilization of debris flows from shallow landslides. Geomorphology, 74: 207–218. DOI：10.1016/j.geomorph.2005.08.013.

Gao Y, Qian H, Yang J, et al. 2016. Laboratory test study on permeability of remolded Malan loess. South- and North- Water Transfers and Water Science & Technology, 14: 7. (in Chinese)

Göksel Türk. 1982. Markov Chain analysis. Mathematical Geosciences, 14: 539–542. DOI：10.1007/bf01077538.

Hallstein J, Metzsch - Zilligen E, Pfaendner R. 2024. Long - term thermal stabilization of poly. Lactic Acid, 17(11): 1996–1944. DOI：10.3390/ma17112761.

Hungr O, Evans SG, Bovis MJ, et al. 2001. A review of the classification of landslides of the flow type. Environmental and Engineering Geoscience, 7: 221–238. DOI：10.2113/gseegeosci.7.3.221.

Jiang Y, Ma Z, Gao Y, et al. A review on the impact of water in accelerated carbonation: Implications for producing sustainable construction materials. Cement and Concrete Composites, 2025, 157. DOI：10.1016/j.cemconcomp.2024.105902.

Jiang Y, Hu X, Liang H, et al. 2023. A physically based model for the sequential evolution analysis of rainfall-induced shallow landslides in a catchment. Water Resources Research, 59: e2022WR032716. DOI：10.1029/2022WR032716.

Konagai K, Karunawardena A, Bandara K N, et al. 2023. Early warning system against rainfall-induced landslide in Sri Lanka. Progress in Landslide Research and Technology, Cham: Springer International Publishing, 1(1): 217–235.

Leng Y, Peng J, Wang Q, et al. A fluidized landslide occurred in the Loess Plateau: A study on loess landslide in South Jingyang tableland. Engineering Geology, 2017: 129–136. DOI：10.1016/j.enggeo.2017.05.006.

Li HX, Han SB, Wu X, et al. 2021. Distribution, characteristics and influencing factors of fresh groundwater resources in the Loess Plateau, China. China Geology, 4(3): 509–526. DOI：10.31035/cg2021057.

Li M, Zhang X, Yang Z, et al. 2020. The rainfall erosion mechanism of high and steep slopes in loess tablelands based on experimental methods and optimized control measures. Bulletin of Engineering Geology and the Environment, 79: 4671–4681. DOI：10.1007/s10064-020-01854-3.

Li PY, Li JH, Wu JH, et al. 2024. Effects of loess-paleosol interbedding on soil moisture transport and soil microstructure. Hydrogeology & Engineering Geology, 51(3): 1–11. (in

Chinese) DOI：10.16030/j.cnki.issn.1000-3665.202403039.

Lu XS, Jiang Y, Wang NQ, et al. 2023. Progressive deformation and failure mechanism of loess fill slopes induce by rainfall: Insights from flume model tests. Bulletin of Engineering Geology and the Environment, 82: 385. DOI：10.1007/s10064-023-03413-y.

Ma JL, Wang Q, Zhong XM, et al. 2025. Experimental analysis of rainfall - induced instability and failure patterns in loess fill slopes. Advances in Civil Engineering, 2025(1): 5233914. DOI：10.1155/adce/5233914.

Nan J, Peng J, Zhu F, et al. 2021. Multiscale characteristics of the wetting deformation of Malan loess in the Yan'an area, China. Journal of Mountain Science, 18: 1112−1130. DOI：10.1007/s11629-020-6490-8.

Peng J, Fan Z, Wu D, et al. 2015. Heavy rainfall triggered loess – mudstone landslide and subsequent debris flow in Tianshui, China. Engineering Geology, 186: 79−90. DOI：10.1016/j.enggeo.2014.08.015.

Peng JB, Wang QY, Zhuang JQ, et al. 2020. Dynamic formation mechanism of landslide disaster on the Loess Plateau. International Journal of Geomechanics, 26: 714−730. (in Chinese) DOI：10.12090/j.issn.1006-6616.2020.26.05.059.

Ren T, Zhu LJ, Pei X, et al. 2021. Study on compression test and mechanism of double polymer double cross - linked solidified loess. Yellow River, 43(6): 140−144. (in Chinese) DOI：10.3969/j.issn.1000-1379.2021.06.028.

Regmi RK, Jung K, Nakagawa H, et al. 2014. Study on mechanism of retrogressive slope failure using artificial rainfall. Catena, 122: 27−41. DOI：10.1016/j.catena.2014.06.001.

Tan Wj, Huang QB, Chen X, et al. 2022. Physical model test on the interface of loess fill slope. Land, 11: 372−1372. DOI：10.3390/land11081372.

Xiao J, Porter SC, An ZS, et al. 1995. Grain size of quartz as an indicator of winter monsoon strength on the Loess Plateau of Central China during the Last 130, 000 Yr. Quaternary Research, 43: 22−29. DOI：10.1006/qres.1995.1003.

Xu Q, Pu CH, Wang XH, et al. 2025. Revealing terrestrial uplift in large-scale land creation areas on the loess plateau using InSAR time series data. Engineering Geology, 347(1): 107946−107946. DOI：10.1016/j.enggeo.2025.107946.

Yang, KH, Thuo JN. 2018. Numerical evaluation of reinforced slopes with various backfill-reinforcement-drainage systems subject to rainfall infiltration. Computers and Geotechnics, 102: 218−227. DOI：10.1016/j.compgeo.2017.10.012.

Yu FD, Qiao G, Wang K, et al. 2023. Investigation of groundwater characteristics and its influence on Landslides in Heifangtai Plateau using comprehensive geophysical methods. Journal of Groundwater Science and Engineering, 11(2): 171−182. DOI：10.26599/JGSE.2023.9280015.

Yu GQ, Wang Q, Zhu LF, et al. 2023. Regulation of vegetation pattern on the hydrodynamic processes of erosion on hillslope in Loess Plateau, China. Journal of Groundwater Science and Engineering, 11(1): 4−19. DOI：10.26599/JGSE.2023.9280002.

Zhang H, Hu C, Liu B, et al. 2003. Mechanical properties experiment of compacted loess - lime. Journal of Traffic Transportation Engineering, 3: 13−16.

Zhang Q, Qian H, Xu P, et al. 2022. Microscale evidence for and formation mechanisms of shear-strength anisotropy of a loess-paleosol sequence since the late Early Pleistocene: The case study of the Xiushidu profile, Southern Chinese loess Plateau. Catena, 213: 106228. DOI：10.1016/j.catena.2022.106228.

Zhang S, Zhang X, Pei X, et al. 2019. Model test study on the hydrological mechanisms and early warning thresholds for loess fill slope failure induced by rainfall. Engineering Geology, 258: 105135. DOI：10.1016/j.enggeo.2019.05.012.

Zhang X, Zhong Y, Pei X, et al. 2021. A cross - linked polymer soil stabilizer for hillslope conservation on the Loess Plateau. Frontiers in Earth Science, 9: 771316. DOI：10.3389/feart.2021.771316.

Zhao ZF, Zhu YP, Ye SH, et al. 2025. Experimental study on the failure characteristics of the

loess high slope under the coupled effects of soil consolidation, rainfall, and evaporation. Engineering Failure Analysis, 171: 109383. DOI：10.1016/j.engfailanal.2025.109383.

Zhou X, Yan Y, Li Y, et al. 2025. Application of cellulose-rich organic resource improves soil quality and plant growth by recruiting beneficial microorganisms. Applied Soil Ecology, 207: 105909. DOI：10.1016/j.apsoil.2025.105909.

Zhu R, Xie W, Liu Q, et al. 2022. Shear behavior of sliding zone soil of loess landslides via ring shear tests in the South Jingyang Plateau. Bulletin of Engineering Geology and the Environment, 81: 267. DOI：10.1007/s10064-022-02719-7.